Supporting Information (Molecular thermodynamic modeling of a bilayer perforation in mixed catanionic surfactant systems, Ksenia A. Emelyanova, Alexey I. Victorov)

I. Estimation of the micellar composition for DTAB / SDS / NaBr system

The pseudophase approach [1] makes possible to calculate the composition of a mixed micelle from the knowledge of the CMC of the individual surfactants, surfactant mixture, and the activity coefficients of surfactants in the micellar pseudophase. Using the model of regular solution with the interaction parameter β for the activity coefficients, we have

$$\begin{cases} x_1^m = \dfrac{x_1 CMC_2 f_2^m}{x_1 f_2^m CMC_2 + x_2 f_1^m CMC_1} \\ \dfrac{1}{CMC} = \dfrac{x_1}{f_1^m CMC_1} + \dfrac{x_2}{f_2^m CMC_2} \\ \ln f_1^m = (x_2^m)^2 \beta \end{cases} \qquad \text{(S1)}$$

where x_1^m and x_2^m are the mole fractions of the 1-st and the 2-nd surfactants in the micelle; x_1 and x_2 are their gross mole fractions in solution calculated on the solvent-free basis; CMC, CMC_1 and CMC_2 are the critical micellar concentrations of the surfactant mixture, and of the individual 1-st and 2-nd surfactants, respectively; f_1^m is the activity coefficient of the 1-st surfactant in the mixed micelle.

For the DTAB / SDS / NaBr in water at 298.15 K, β = -25.5. [2, 3] CMC_{SDS} = 8 mM (no added salt) and 1.5 mM (0.1 M NaCl). CMC_{DTAB} = 14.5 mM (no added salt) and 4.5 mM (0.1 M NaBr). [4] Experimental CMC of DTAB / SDS mixture [5] are given in Tab. S1 together with micellar compositions calculated from Equations S1. These compositions are shown in Fig. 3A (black symbols).

Table S1. Experimental CMC for DTAB / SDS aqueous mixture at 298.15 K (no added salt) [5] and calculated micellar composition (mole %).

DTAB:SDS in solution	CMC mM	DTAB:SDS in micelles
30:70	1.8	36:64
32:68	1.9	35:65
35:65	2.1	34:66

II. Evolution of the optimal dimensions of pore's toroidal rim in mixtures of cationic and anionic surfactants

Fig. S1 shows calculated optimal minor radius b of toroidal rim of the pore in a symmetrical mixture: DTAB + anionic surfactant that has the same length of the tail and the head cross-sectional area, viz., $n_c(1) = n_c(2) = 12$ and $a_p(1) = a_p(2) = 0.54\ \text{nm}^2$. The optimal major toroid's radii (in units of b) are shown in Fig. S2. Depending on the aggregate composition, the toroid of the optimal dimensions may be either thermodynamically stable or become metastable when aggregates of other shape have lower aggregation free energy. Fig. S2 shows composition intervals of stable cylinders and non-perforated lamellae, as explained below. Shown in Fig. S3, are the average area per surfactant head and different contributions to the aggregation free energy of the optimal toroidal rim.

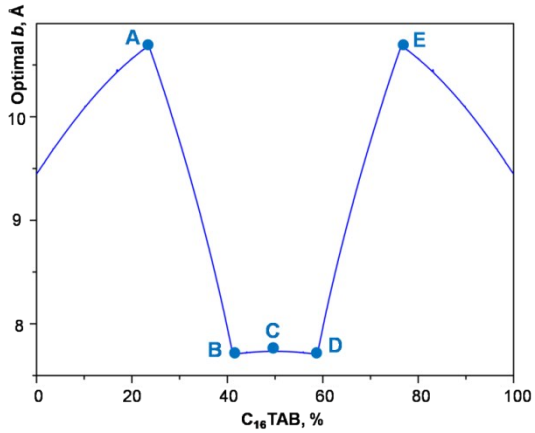

Figure S1. Optimal minor radius b of the pore's toroidal rim *vs* composition of the aggregate (mole %) in a symmetrical mixture of DTAB with an oppositely charged (anionic) but otherwise identical surfactant. T = 298.15 K, 0.1 M added salt.

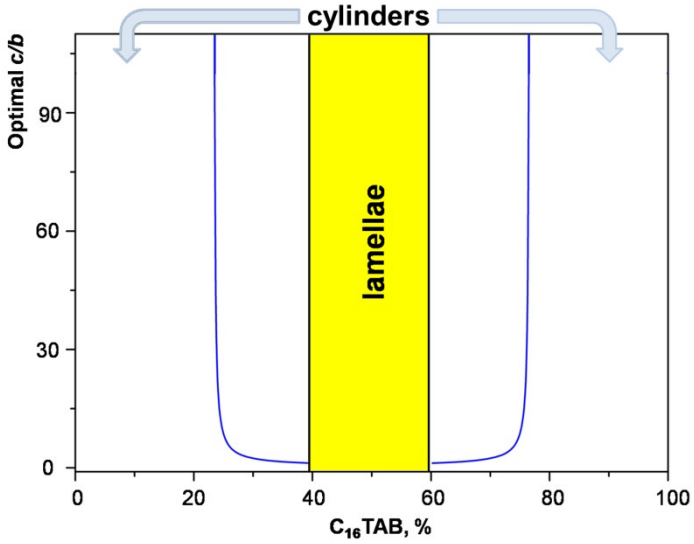

Figure S2. Optimal ratio of toroid's radii *vs* its composition for symmetrical catanionic mixture (explained in the caption to Fig. S1). For large c/b, the toroid transforms into cylinder with the same b and infinite c. Zone of stable nonperforated lamellae predicted by the model is shown in yellow.

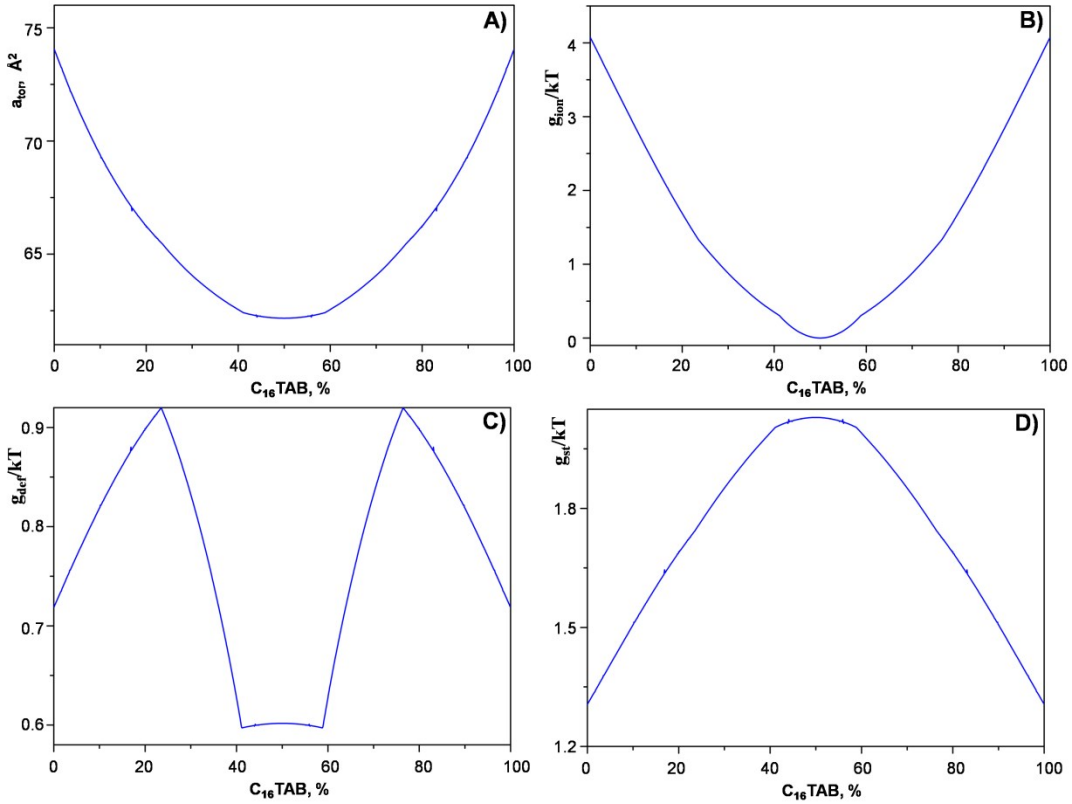

Figure S3. Effects of the catanion aggregate's composition on the average area per surfactant head (A) and on the contributions to the free energy of aggregation: electrostatic term (B), deformational term (C) and steric repulsion term (D). Same system as in Figs. S1, S2.

Large interfacial contribution to the aggregate free energy always favors smaller area per surfactant head. This is opposed by the electrostatic repulsion of the charged heads that always prefers lower surface charge density. As we start adding DTAB to a purely anionic aggregate, the surface charge density is reduced so strongly through the partial compensation of charge that the ionic contribution to the free energy decreases, Fig. S3B, despite the reduction of the surface area, Fig.S3 A, driven by the interfacial term. Nevertheless for low to medium concentration of DTAB, the electrostatic repulsion of heads is strong enough to disfavor the negative curvature of the toroidal pore (in the plane of its major radius) and the optimal structure is the cylinder, i.e. the limiting case of toroid with an infinitely large c/b, Fig. S2. The area per molecule in the toroid is related to its radii [6]

$$a = \frac{\left(\frac{\pi}{2}\frac{c}{b} - 1\right)}{b\left(\frac{\pi}{2}\frac{c}{b} - \frac{1}{3}\right)} v_{tail} \qquad \text{(S2)}$$

where v_{tail} is the volume per surfactant tail in the core (that does not change with the composition in a symmetrical mixture). At very large c/b this area is inversely proportional to b and the

reduction of the area implies an increase of b, the radius of the optimal cylindrical aggregates as shown in the left part of Fig. S1 up to point A. Upon reaching this point the situation changes dramatically. The surface charge is compensated enough to make possible the combination of an unfavorable negative curvature, c^{-1}, with a favorable (and substantially larger) positive curvature b^{-1} in the toroidal rim. As we continue adding DTAB to the aggregate, the optimal c/b ratio rapidly falls off (Fig. S2). This falloff controls the further reduction of the surface area, Fig.S3A, notwithstanding substantial decrease in b (Fig. S1, from point A to point B) that is favored by both toroid's electrostatics (Fig. S3B) and the deformation of surfactant tails preferring less extended conformation, Fig. S3C. It is the composition interval between points A and B of Fig. S1, where we find the stable bilayer pores of a finite diameter, see Fig. S2.

As c approaches b upon further addition of DTAB, Fig. S2, the ratio of the brackets in Eq. (S2) levels off and the further minor decrease of the area per surfactant chain (Fig. S3A) is due to a minor increase in b from point B to point C in Fig. S1. In this compositional zone the electrical charge of the aggregates approaches zero and nonperforated lamellae become the preferred morphology (Fig.S2) owing to a beneficial tail-deformation term. [7]

The steric repulsion of surfactant heads always prefers large area per chain, Fig. S3D. Nevertheless it is totally overwhelmed by the interfacial term for large enough areas considered in this example.

For concentration of DTAB beyond the equimolar composition, the behavior of a symmetrical mixture is the mirror image of its behavior below the equimolar composition (point C in Fig. S1).

Stable perforations may form in two regions: A – B and D – E.

Our model shows how the asymmetry in the molecular parameters of surfactants distorts the symmetrical response of the pore dimensions to the change of composition and /or salinity. This is illustrated in Figs. S4 and S5 for the C_{16}TAB / SOS / NaBr and in Fig. S6 for a model catanionic mixture.

The dependence of b on the aggregate composition, Fig.S4, is qualitatively similar to that for the symmetric mixture (Fig. S1). Apart from the trivial difference in the thickness b of cylindrical aggregates that contain pure surfactants, Fig. S4 shows smaller drop of the pore thickness for pores enriched in the shorter chain surfactant (zone A – B) than for the pores enriched in the longer chain surfactant (zone E – D). Fig. S6 shows similar results for a model surfactant mixture where, in contrast to C_{16}TAB / SOS system, the longer tail surfactant has much smaller head than the shorter chain surfactant. Such behavior is confirmed by calculations performed for many other combinations of surfactants differing in chain length and head cross sectional areas.

Our model predicts that upon increasing concentration of the deficient surfactant in the catanionic mixture both the diameter and the thickness of the stable pore may only decrease.

The effect of solution salinity is illustrated in Fig. S3. For low salinity, weakly screened electrostatic interactions dominate and the behavior of the system is less surfactant-specific.This results in a more symmetrical b -composition curve than that for high salinity, Fig. S4.

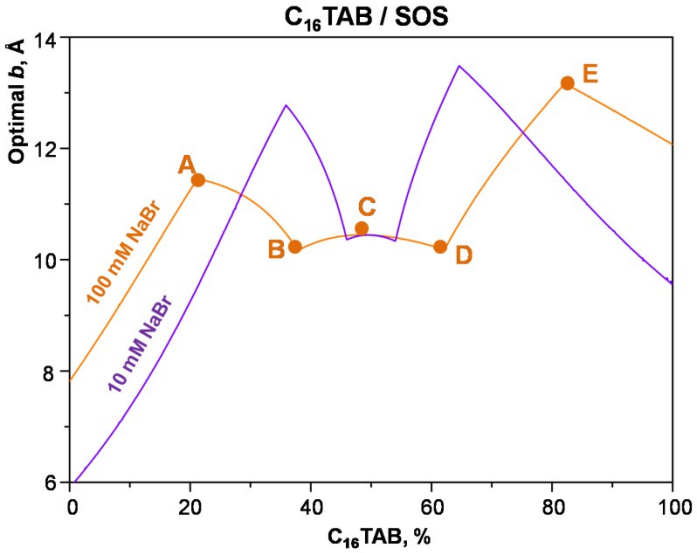

Figure S4. Optimal minor radius *b* of the pore's toroidal rim *vs* composition of the aggregate (mole %) for the C_{16}TAB / SOS / NaBr aqueous mixture. T = 298.15 K. $a_p(C_{16}TAB) = 0.54$ nm^2, $n_c(C_{16}TAB) = 16$, $a_p(SOS) = 0.17$ nm^2, $n_c(SOS) = 8$

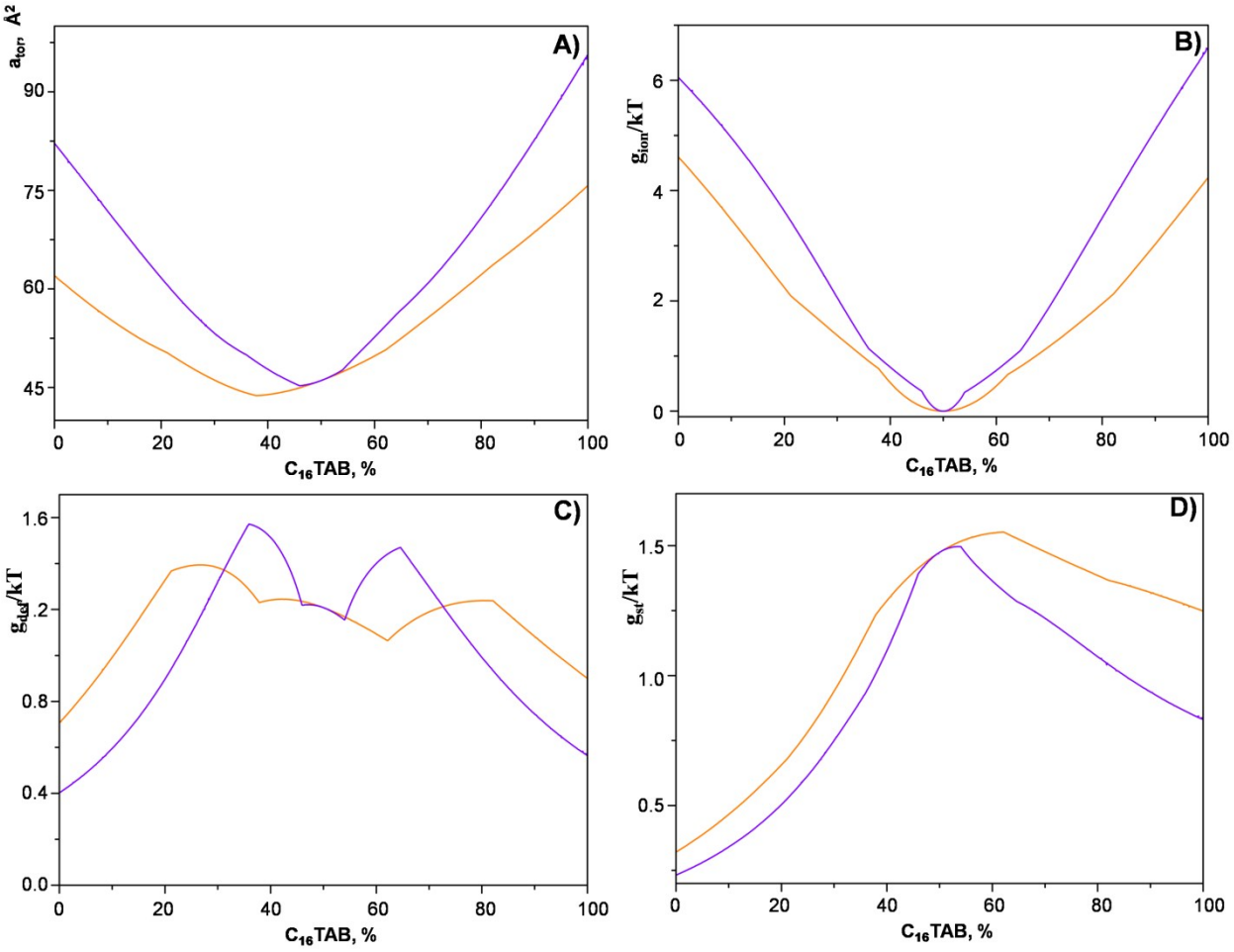

Figure S5. Effects of the aggregate's composition on the average area per surfactant head (A) and on the contributions to the free energy of aggregation: electrostatic term (B), deformational term (C) and steric repulsion term (D). C_{16}TAB / SOS / NaBr system, 0.01 M and 0.1 M added salt, T = 298.15 K.

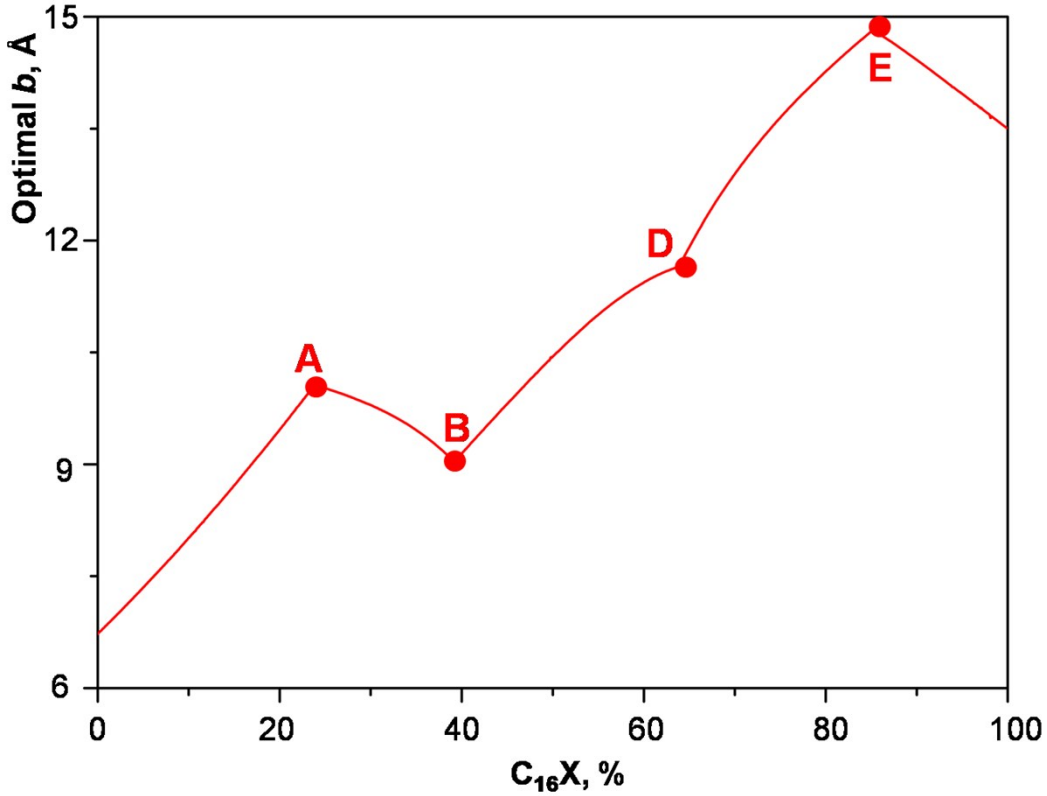

Figure S6. Optimal minor radius b of the pore's toroidal rim vs composition of the aggregate (mole %) containing long-chain cationic surfactant $C_{16}X$ with small head (a_p = 0.17 nm^2) and short-chain anionic surfactant $C_{12}Y$ with large head (a_p = 0.54 nm^2). T = 298.15 K, 0.1 M of salt.

REFERENCIES

1) Holmberg, K.; Jonsson, B.; Kronberg, B.; Lindman, B. Surfactants and polymers in aqueous solution.2-nd ed. John Willey & Sons, Ltd, **2002**.Chapter 5.Mixed micelles.

2) Holland P. Mixed surfactant systems, P. M. Holland, D.N. Rubingh (Eds), ACS Symposium series, № 501; American Chemical Society, Washington, DC, **1992**, p. 41.

3) Zhu, B.Y.; Rosen, M.J. *J. of Colloid & Interface Sci.***1984**, *99*, 435.

4) Mukerjee, P.; Musels, K. J. Critical micelle concentration of aqueous surfactant systems. NSDS - Nat. Bur. Stand. **1971**.

5) L.G. Chen; H. Bermudez.*Langmuir***2008**, 29, 2805 - 2808.

6) Victorov, A. I.;Plotnikov, N.V.; Hong, P.-D. Molecular thermodynamic modelingofthe morphology transitions in a solution of a diblock copolymer containing a weak polyelectrolyte chain.*J. Phys. Chem. B***2010**, *114*(27), 8846–8860.

7) Emelyanova, K. A.; Victorov, A. I. Driving force for spontaneous perforation of bilayers formed by ionic amphiphiles in aqueous salt. *Langmuir***2017**, *33*, 13438-13443.